Effect of oxidation of the ultrathin Fe electrode material on the strength of magnetoelectric coupling in composite multiferroics

M. Fechner,[1,*] S. Ostanin,[1] and I. Mertig[1,2]
[1]*Max-Planck-Institut für Mikrostrukturphysik, Weinberg 2, D-06120 Halle, Germany*
[2]*Fachbereich Physik, Martin-Luther-Universität Halle-Wittenberg, D-06099 Halle, Germany*
(Received 13 May 2009; revised manuscript received 23 July 2009; published 11 September 2009)

We present an *ab initio* study of the effect of iron oxidation on magnetoelectric coupling which appears at the ferromagnet/ferroelectric interface, such as $Fe_2/ATiO_3(001)$ (A=Ba,Pb). The oxygen coverage, c, ranging between one half and two adsorbed O per each Fe atom was simulated within a slab geometry. Since the change in magnetization induced by electric polarization reversal remains robust below $c<3/2$, we suggest that the surface oxidation of composite multiferroics will not significantly damage their switchable magnetoelectricity.

DOI: 10.1103/PhysRevB.80.094405 PACS number(s): 75.80.+q, 77.84.Lf, 68.47.Gh, 73.20.At

I. INTRODUCTION

When any two of all four primary ferroic properties, i.e., ferroelectricity, ferromagnetism, ferroelasticity, and ferrotoroidicity coexist in the so-called multiferroic material[1] (MF), its symmetry is dramatically restricted.[2] In the absence of space-inversion and time-reversal symmetry, the occurrence of ferroelectricity and ferromagnetism in the same phase of a MF allows the observation of both a switchable electric polarization, **P**, and a switchable magnetization **M**. This phenomenon, in principle, allows to store information in nanometer-sized memories with four logic states.[3–5]

Although some single-phase MFs, such as $BiFeO_3$ and $RMnO_3$ (R: rare earths), were studied since the seventies, the search for novel multiferroics is not finished.[6] Moreover, their classification, which is based on the different mechanisms of induced polarity, has been revised since 2003 (see Ref. 7, and references therein) when the type-II class of magnetic MF was established. The type-I class of multiferroics contains numerous perovskitelike materials in which ferroelectricity and magnetism appear independently of one another and where **P** appears at higher temperatures than **M**. One can find several subclasses of type-I MF depending on the mechanism of their ferroelectricity.[7] In a type-II MF, ferroelectricity is driven by the electronic order degrees of freedom related to spin arrangements which break inversion symmetry. This symmetry breaking occurs due to a spin-orbit-related mechanism in conjunction mostly with the spin-spiral magnetic structure. For instance, this happens in $TbMnO_3$ below 28 K when the Mn spin tips sweep out a cycloid. Such cycloidal spin arrangement via the Dzyaloshinskii-Moria antisymmetric exchange creates a polarization: $\mathbf{P}\sim\mathbf{r_{ij}}\times[\mathbf{S_i}\times\mathbf{S_j}]$, where $\mathbf{r}_{ij}$ is the vector connecting neighboring spins $\mathbf{S}_i$ and $\mathbf{S}_j$. There is another subclass of the type-II multiferroics where ferroelectricity may appear for some collinear antiferromagnetic structures below the Néel temperature due to the Heisenberg-type symmetric exchange. Thus, ferroelectricity of the type-II MF is caused by a particular type of magnetic order, which exists only at low temperature and which is predominantly antiferromagnetic.

In multiferroics, no matter what its class is, an applied electric field, **E**, displacing the magnetic ions, may affect the magnetic exchange coupling or, vice versa, the external magnetic field, **H**, induces the electric polarization: $P_i\sim\alpha_{ij}H_j$, where α_{ij} is the magnetoelectric tensor and $(i,j)=x,y,z$. According to the Landau theory, the linear magnetoelectric[1] (ME) contribution to the Gibbs free energy is $\alpha_{ij}E_iH_j$. If α is sufficiently strong then **M** can be easily modified by **E**. It should be kept in mind that magnetoelectricity is an intrinsic bulk property for which the induction of **M** depends linearly on **E**. In the type-I single-phase MF, **P** and **M** weakly interact with each other and, therefore, α is marginal there. Besides, all these multiferroics possess a hierarchy of phase transformations,[8] where the magnetism disappears far below room temperature. In a type-II MF, the magnitude of **P** is never large. However these materials disclose a relatively large ME coupling. For instance, the direction of **P** in $TbMnO_3$ may flop by 90° when an applied magnetic field forces the plane of a magnetic cycloid to rotate by 90°. Obviously, the quest for fundamentally new multiferroics requires a better understanding of the mechanisms which mediate the ME coupling.

Ab initio calculations based on the density-functional theory (DFT) predict that a ~30 meV voltage, applied across the $SrRuO_3/SrTiO_3$ interface, with no magnetic cations, can induce a net magnetic moment.[9] Since the space-inversion symmetry is broken between the two unlike terminations, the ME effect results entirely from spin accumulation at the interface. The effect might be enhanced by the use of materials with higher spin polarization. Indeed, a more robust scenario of magnetoelectricity occurs in epitaxially grown two-phase MF consisting of ferroelectric and ferromagnetic components where the ME effect is mediated by strain across the biferroic interface. Inaccessible by conventional synthesis, composite MF exhibit specific properties which are superior to those of customary materials. The *ab initio* studies suggest that chemical bonding at the $Fe/BaTiO_3(001)$ interface is the source of strong ME coupling.[10,11] The interfacial Ti atoms show an induced magnetic moment of about 0.3 μ_B. Moreover, for the two opposite directions of **P** ($P_\downarrow$ and $P_\uparrow$), there are rather noticeable differences of 0.1–0.2 μ_B in the magnetic moments of Fe and Ti at the interface. This is a very promising phenomenon, which is entirely confined to the ferroelectric/ferromagnetic

interface and which is different from the bulk ME effect. The interface ME effect defines the change in magnetization at the coercive field E_c: $\mu_0 \Delta M \approx \alpha E_c$. The α of $\sim 2 \times 10^{-10}$ G cm^2/V estimated for Fe/$BaTiO_3$(001) from first principles, is two orders of magnitude larger than that predicted for $SrRuO_3/SrTiO_3$.

Epitaxial growth of the two-phase MF thin films of high quality continues to be very challenging. A 30-nm-thick Fe(001) film has been grown recently on a ferroelectric $BaTiO_3$(001) substrate.[12] For this MF composite, the interface ferromagnetic resonance mode is characterized by a large out-of-plane magnetic anisotropy comparable and opposite in sign to the shape anisotropy, which favors the in-plane easy axis for the thick-film interiors. The trends of magnetic anisotropy detected for Fe/$BaTiO_3$ are in a good agreement with the corresponding *ab initio* calculations.[11,13] In the case of one Fe monolayer (ML), the DFT predicts that perpendicular anisotropy is favored to in-plane anisotropy by 0.72 meV (0.54 meV) per Fe atom for $P_\downarrow$($P_\uparrow$).[11] Although the spin reorientation transition under switching of **P** is not found from first principles, the ME coupling alters the magnetocrystalline anisotropy energy by $\sim$50%. The magnetic order of Fe/$BaTiO_3$ can be tuned by the Fe layer thickness to almost zero-**M** ferrimagnetic upon deposition of a second Fe ML.[11] Ferromagnetic order is restored for the Fe films thicker than 3 ML where the shape anisotropy energy favors in-plane alignment of **M**.[13]

Recently, Niranjan *et al.*[14] modeling the two different $Fe_3O_4/TiO_2/BaTiO_3$(001) interfaces, within the DFT, have found that ME coupling is stronger for the O-deficient type of the Fe_3O_4 interface. The O-deficient termination of Fe_3O_4 contains Fe cations on tetrahedron sites, whereas the FeO_2-terminated magnetite surface contains Fe on octahedron sites in addition to oxygen anions. These interface O atoms reduce the hybridization between Fe and Ti thus decreasing the magnetic moment induced on Ti. This leads to the reduction in the ME effect for the O-rich Fe_3O_4/TiO_2 interface since its magnetoelectricity is primarily controlled by the Ti magnetic moments. Therefore, the presence of extra oxygen or oxygen vacancies at the biferroic interface plays an important role. The temperature-dependent magnetization curves of epitaxial magnetite films grown on $BaTiO_3$(001) demonstrate[15] a strong perpendicular magnetic anisotropy, which is modified by the piezoelectric response of the substrate.

So far, the *ab initio studies* of composite MF were focused on their perfect interfaces with no oxidants. However, the strength of the ME interface effect may be very sensitive to the degree of oxidation. The Fe oxidation is unavoidably motivated, first, by the growth process of the ferroelectric since oxygen remaining in the chamber will react with iron during its growth. Second, for the uncovered Fe films further oxidation occurs when the sample is removed from the chamber. These two possible scenarios may result in some particular Fe-O compositions, which vary from highly oxidized Fe to an almost clean surface. Thus, the *ab initio* based modeling would be extremely useful. In this work, we study from first principles the key electronic, magnetic, and structure factors behind the oxidation process of the 1 ML Fe grown on $BaTiO_3$(001) and $PbTiO_3$(001). We demonstrate in which positions oxygen adatoms sit above the Fe layer and that the ME coupling is robust against the O adsorption.

II. METHOD

Our DFT calculations were performed within the local spin-density approximation, using the projector-augmented wave (PAW) pseudopotentials and a plane-wave basis cutoff energy of 650 eV, as implemented within the Vienna *ab initio* simulation package (VASP).[16,17] To model the (001) surface of $BaTiO_3$ (BTO) and highly polar $PbTiO_3$ (PTO), we constructed the 25-atom and 5-unit-cell ($\sim$2-nm)-thick perovskite supercell, with a vacuum spacer of 2 nm in the [001] direction. The lattice parameters were set to the equilibrium values of tetragonal ABO_3 (A=Ba and Pb and B=Ti).[18] For BTO (PTO), the in-plane lattice parameter, a, is 3.943 Å (3.858 Å) and c/a=1.013 (1.071). The corresponding bulk polarization values, calculated by the Berry phase approach[19,20] for BTO and PTO, are 0.23 and 0.94 C/m^2, respectively. The Ti/O displacements occurring in tetragonal PTO and BTO cause the direction of **P** along [001]. When **P** is antiparallel to the surface normal ($P_\downarrow$), oxygen is placed above the cations in each ML, and vice versa, the configuration $P_\uparrow$ means that all intralayer displacements $\delta = z_O - z_{cation} < 0$. Since the (001) surface of ABO_3 is TiO_2 terminated[18] for both directions of **P**, we study the Fe_2/TiO_2/BTO(001) and Fe_2/TiO_2/PTO(001) interfaces where the Fe atoms find their relaxed positions atop oxygen, as shown in Figs. 1(a) and 1(b). This is in agreement with previous *ab initio* calculations.[10,11]

The equilibrium bond length calculated for molecular O_2 is 1.23 Å. For $Fe_2/TiO_2/ATiO_3$(001), the in-plane lattice parameter is about 3.9 Å while the Fe-Fe separation is $\sim$2.75 Å. The latter is two times larger than that of the O_2 dissociation. Thus, to model the Fe oxidation of Fe/BTO and Fe/PTO we consider O coverages, $c(O_x:Fe_2)$, ranging between c=1/2 and two adsorbed O atoms per Fe atom (c=2). There are 12 possible configurations shown in Fig. 1(c). For c=0.5, one oxygen adatom per unit cell can occupy the site either above A or above Ti or, alternatively atop Fe. For c=1, the two O adatoms form four configurations marked in Fig. 1(c) as AT, AF, TF, and FF. In the case of c=1.5, we relax the ATF, TFF, and AFF configurations and, finally, for c=2 there are two more possibilities to distribute four adatoms, such as ATFF (the case of full coverage) and 4H, which means that all four hollow sites are occupied by O. Using the $10 \times 10 \times 6$ Monkhorst-Pack[21] k-point mesh for the Brillouin-zone integration, we relaxed the O adatoms and Fe atoms plus all atoms of the two top ABO_3 unit cells until the forces were less than 1.0×10^{-2} eV/Å. After relaxation we found that oxygen adatoms for all coverages except c=2 form an overlayer above the Fe layer with the distance depending on the coverage and direction of **P**. The total and site-projected partial density of states (DOS) as well as the local magnetic moments were calculated within the PAW option of VASP using the tetrahedron method and a dense k-point mesh. Additionally, to verify the calculated magnetic moments we varied the Wigner-Seitz radii of each atomic species in the cell. For c=0, the local moments calculated by

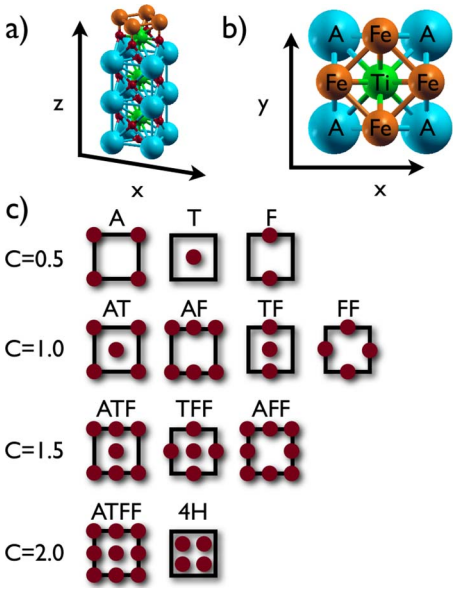

FIG. 1. (Color online) Unit cell of oxidized biferroic $O_x/Fe_2/TiO_2/ATiO_3(001)$ (A=Ba,Pb), with a 2-nm-thick vacuum layer. The top layers of the clean biferroic system (x=0), are plotted as side view and top view in panel (a) and (b), respectively. The lower panel (c) shows the O adatom positions, which mimic the oxygen coverage, $c(O_x:Fe_2)$, ranging between $c=1/2$ and two adsorbed O per Fe atom. For $c=1/2$, we relaxed the configurations marked with the labels A, T, and F, where an oxygen adatom can occupy any site above A, Ti, or Fe, respectively. In the case of $c=1$ ($c=3/2$), there are four (three) such configurations and, finally, for $c=2$ we consider a pair of possibilities, one of which marked as 4H means that all four hollow sites are occupied by O.

VASP are in good agreement with those of our previous work[11] in which another DFT code, the multiple-scattering Korringa-Kohn-Rostoker method, was used.

III. RESULTS AND DISCUSSION

In our study of an uncovered ML Fe on $ABO_3(001)$, we have found[11] a strong ferromagnetic order of the Fe layer with a magnetic moment of $\approx 3\ \mu_B$. The reversal of the electric polarization induces a change in the total magnetization $\Delta M=M(P_\downarrow)-M(P_\uparrow)$ of 1 μ_B (0.05 μ_B) for Fe/PTO (Fe/BTO). This is mostly due to the interfacial-Ti magnetic moment, aligned antiparallel to that of Fe and originated from the hybridization of Ti $3d$ with minority-spin Fe $3d$ states. Reversal of **P** affects the hybridization making it stronger for $P_\downarrow$ when the distance between Fe and Ti becomes slightly shorter.

A. Structural optimization

In Fig. 2, we plot the total energy of $O_x/Fe_2/ATiO_3$ (A=Ba,Pb and $1\leq x\leq 4$) for the two polarization directions and for each of the oxygen coverages between $c=0.5$ ($x=1$) and $c=2$ ($x=4$). The O configurations are labeled as shown in Fig. 1. For each c between 0.5 and 2, the lowest energy configuration is the zero energy. In the case of $c=0.5$, the most favorable is the configuration A. The difference in energy between the configurations A and T for this O coverage is $E_T-E_A\sim 0.2$ eV. For the two ABO_3 substrates, the energetics are almost the same while the **P** reversal yields the energy differences compatible with that of E_T-E_A. When the O atom relaxes above Fe this results in the highly unfavorable configuration F, with the energy of 2.1 eV above that of case A. It can be understood by inspecting the relaxed structure of the A and T configurations. We find them very similar to that of a O/Fe(001) film, which were debated many times in the literature[22] and where the O adatom is relaxed at the hollow site ~ 0.3 Å above the Fe ML. The configurations A and T show no significant change with respect to each other and with respect to an uncovered ML Fe on ABO_3. In the case of configuration F, the coverage $c=0.5$ makes the two Fe sites nonequivalent and, as a result, the Fe atom below oxygen moves outward the Fe layer, displacing therefore the O atoms of the interface TiO_2 layer in the same way. The structural distortions make the configuration F energetically unfavorable.

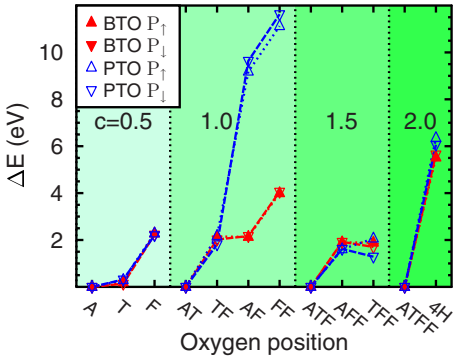

FIG. 2. (Color online) The total energy of $O_x/Fe_2/ATO_3(001)$ (A=Ba,Pb and $1\leq x\leq 4$) is plotted for the 12 relaxed O configurations which are shown in Fig. 1. For each coverage c, the lowest energy configuration is the zero energy.

The energetics which is calculated for the coverage $c=1$ can be explained using our findings for $c=0.5$. We expect the two O adatoms occupy the positions above A and Ti. Here, the **P** reversal gives a change in energy of about 0.2 eV for both systems. Any of the three other configurations: TF, AF, or FF always includes at least one energetically unfavorable position atop Fe that drastically increases the corresponding surface energy. The configuration FF after relaxation represents the case of the most distorted system, which energy is larger by 12 eV (4 eV) compared to that of the AT configuration of PTO (BTO). For the same reason, the energetically favorable scenario of $c=1.5$ is the configuration ATF when one site above Fe is empty. Regarding $c=2$, we have inspected two configurations: ATFF and 4H, which are shown in Fig. 1. It turns out that the 4H configuration, with all four hollow sites occupied by O, is unfavorable.

In Fig. 3 we plot the intralayer separation between the perovskite O and A/B cation along [001]: $\delta=z_O-z_{cation}$, obtained after relaxation in $O_x/Fe_2/ABO_3(001)$ for the most favorable configuration of each coverage. The adatom configurations A, AT, ATF, and ATFF were chosen for $0.5\leq c\leq 2$. The layers toward the perovskite bulk, starting from the outermost TiO_2 layer, are labeled I, I-1, I-2, etc. The δ ob-

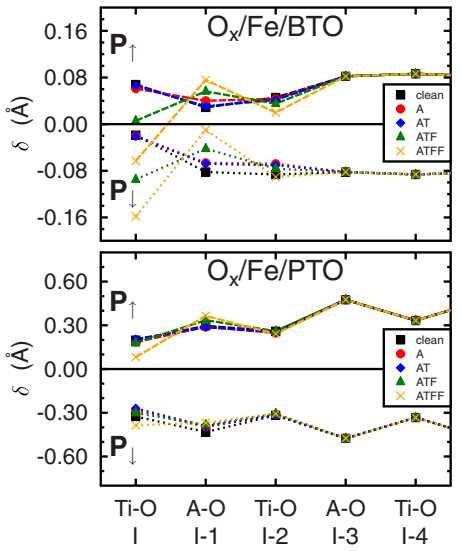

FIG. 3. (Color online) Intralayer atomic displacements $\delta = z_O - z_{cation}$ (in Å) are plotted for several perovskite layers of $O_x/Fe_2/ATiO_3(001)$ (A=Ba,Ti and x=0,1,2,3,4). The outermost TiO_2 layer of the ferroelectric is denoted I and the layers toward the perovskite bulk are labeled I-1, I-2, etc. For each O coverage $c \leq 2$ the lowest energy configuration (A, AT, ATF, and ATFF) was chosen.

tained for $c=0$ are shown in Fig. 3 for comparison. The asymmetry of δ seen between $P_\downarrow$ and $P_\uparrow$ for the layers I, I-1, and I-2 as well as the magnitude of δ, which gradually decreases toward the interface, demonstrate the effect of the depolarizing field and its screening. The effect of oxidation which, in general, should provide less screening, may allow for a depolarizing field to reduce the magnitude of polarization. Here, we detect that for highly polar PTO the effect of oxidation is insignificant, except the O coverage $c=2$. For BTO, this effect also plays no significant role when we exclude the two scenarios of excessive coverage: $c=3/2$ and $c=2$. When $c \leq 1$, the reduction in **P** is noticeable near the interface, however, the ferroelectrically dead layer is not seen there.

The most favored O coverage can be estimated using the calculation of adsorption energy,[23] which is defined as $E_{ad} = (E_{oxid} - E_{clean} - c \cdot E_{O_2})/x$. Here, $E_{oxid} - E_{clean}$ is the energy difference between the oxidized and clean surfaces of Fe_2/ABO_3, E_{O_2} is the energy of the O_2 molecule and x is the

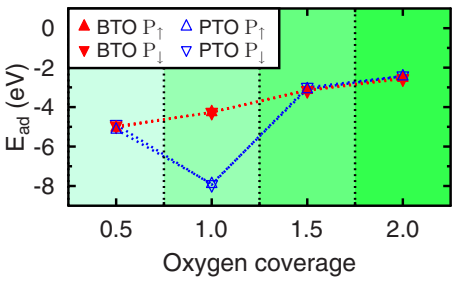

FIG. 4. (Color online) Adsorption energy of $O_x/Fe_2/ATiO_3(001)$ (A=Ba,Pb and x=1,2,3,4) plotted as a function of $c=x/2$.

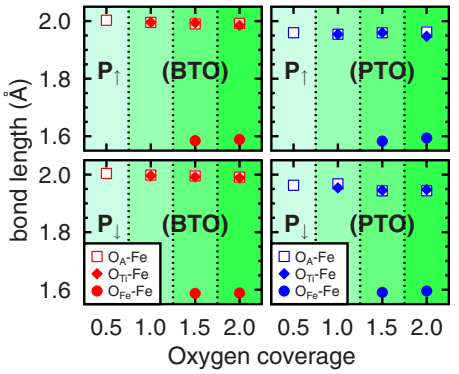

FIG. 5. (Color online) Ionic bond lengths between Fe and oxygen adatoms in $O_x/Fe_2/BTO$ and $O_x/Fe_2/PTO$. The configurations with adatoms above A, Ti, and Fe were used. When $c=2$ the O_A and O_T adatoms find their relaxed positions below the Fe layer.

number of oxygen adatoms. In Fig. 4, we plot the adsorption energy of $O_x/Fe_2/ATO_3(001)$ (A=Ba,Pb and $1 \leq x \leq 4$) versus the O coverage, $c=x/2$, between 0.5 and 2. For the PTO substrate, there is a pronounced minimum of E_{ad} seen in Fig. 4 at $c=1$. The **P** reversal shows a minor effect regardless of the substrate. However, in the case of $O_x/Fe_2/BaTiO_3(001)$,

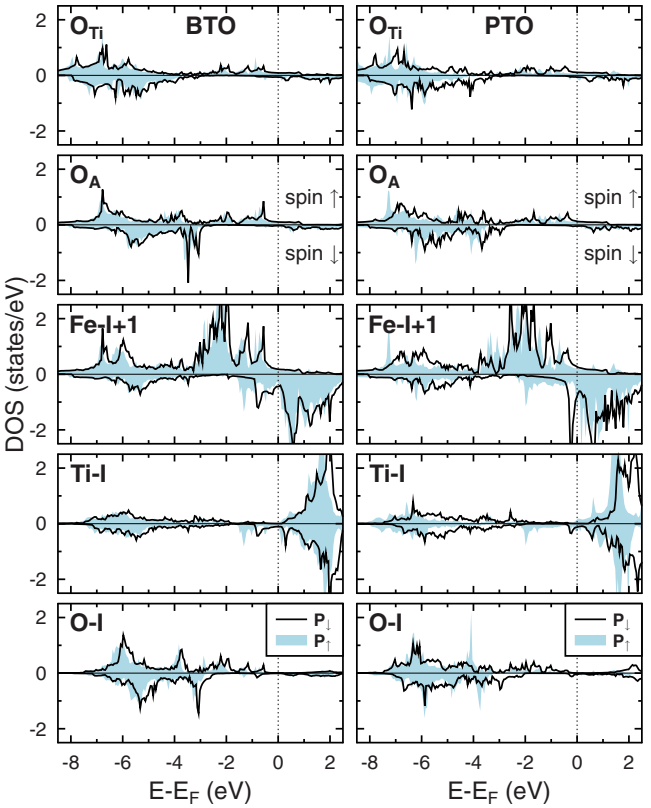

FIG. 6. (Color online) The spin-resolved DOS at the TiO_2-terminated interface of $O_2/Fe_2/BTO(001)$ (left) and $O_2/Fe_2/PTO(001)$ (right). The DOS projected on the O adatoms O_A and O_{Ti} are plotted in the two top panels. The middle panel shows the Fe local DOS while the two lower panels show the DOS calculated for the interfacial Ti and O atoms. Solid lines and shaded plots are the DOS for the polarization $P_\downarrow$ and $P_\uparrow$, respectively. The vertical line indicates the Fermi energy.

TABLE I. Local magnetic moments m_i (in μ_B) calculated for the Fe atom, interfacial Ti-I and O-I and O adatoms of $O_x/Fe_2/TiO_2/ATiO_3(001)$ (A=Ba,Pb and x=0,1,2). The two O adatoms above the Ti and A sites are labeled as O_T and O_A.

	$x=0$		$x=1$		$x=2$	
m_i	$P_\downarrow$	$P_\uparrow$	$P_\downarrow$	$P_\uparrow$	$P_\downarrow$	$P_\uparrow$
			$O_x/Fe_2/BTO$			
O_T					0.21	0.19
O_A			0.20	0.20	0.26	0.27
Fe	2.81	2.83	2.91	2.85	3.21	3.18
Ti-I	−0.22	−0.30	−0.24	−0.34	−0.18	−0.26
O-I	0.08	0.09	0.11	0.10	0.11	0.11
			$O_x/Fe_2/PTO$			
O_T					0.23	0.13
O_A			0.22	0.19	0.24	0.24
Fe	2.87	2.63	3.03	2.66	3.13	2.91
Ti-I	0.00	−0.35	−0.01	−0.39	−0.01	−0.29
O-I	0.10	0.04	0.14	0.07	0.12	0.08

the adsorption energy is rather smooth with no minimum between $0.5<c<2$. It seems that the BTO substrate tends to favor the low c values, namely, $c=0.5$.

The dissimilar behavior of PTO and BTO at the metal interface has been recently studied from first principles by Stengel *et al.*,[24] who analyzed the structure with the use of the ionic bond lengths. Concerning the difference seen in Fig. 4 between the two substrates, a simple explanation can be done by inspecting the O-Fe bond lengths for the O adatoms.

In Fig. 5, we plot the equilibrium O-Fe distances calculated for $O_x/Fe_2/ATiO_3(001)$. Comparing the two systems, the O-Fe separation is always shorter in O/Fe/PTO than in O/Fe/BTO, indicating that the O-Fe bond is stronger in the former system. In particular, for the PTO substrate and coverage $c=1$, the bond length of 1.96 Å between oxygen adatom and Fe is about 0.04 Å shorter than that of the BTO substrate. It seems that oxygen adatom on top of Fe/BTO is weakly bonded to Fe as compared to the Fe/PTO system. This can cause the dissimilarity of PTO and BTO seen in their E_{ad}. The effect of **P** reversal on the O-Fe bond is minor, as shown in Fig. 5. When the O coverage becomes denser, some visible variations in the bond lengths may occur. It should be noted that for the coverages $c=1.5$ and $c=2$, i.e., when extra O adatoms occupy the sites above Fe, this results in relatively short bond lengths of about 1.6 Å. This bond length also varies insignificantly with increasing $c>1.5$. Interestingly, in the case of $c=2$ oxygen atoms, which might occupy the positions above A and Ti, move inward and find their relaxed positions below the Fe layer at nearly the same distance of ~1.95 Å to Fe as those of O_A/O_T adatoms of less dense c.

B. Magnetic properties and magnetoelectric coupling

The spin-resolved and site-projected DOS of $O_2/Fe_2/BTO$ and $O_2/Fe_2/PTO$ for the coverage $c=1$ are plotted in Fig. 6. We show the local DOS calculated for the interfacial Fe, Ti-I, O-I, and two O adatoms. At the interface, we detect metallic behavior. The electronic hybridization between the Fe 3d, Ti 3d, and O 2p states induces magnetic moments at the interfacial Ti-I and O-I. In particular, the Ti moments, aligned antiparallel to those of Fe and O-I, originate from the hybridization of Ti 3d with minority-spin Fe 3d states. For bulk BTO/PTO as well as for BTO/PTO blocks distant from the interface, we obtained a fundamental band gap of about 2 eV while the unoccupied Ti d states form the lower conduction band. It is well known that *ab initio* calculations within the LDA tends to underestimate the band gap of polar perovskites. When theory goes beyond LDA this does not affect the empty conduction band whereas the metalliclike DOS at the interface together with the band gap can be quantitatively affected. As the result, the magnetic contributions to the ME effects coming from the Ti-I and Fe atoms might be slightly disproportionally changed compared to those of the LDA calculation. We believe, however, that the impact of electronic correlations is minor here.

For the two dually polar $O_x/Fe/ATiO_3(001)$ systems and $x\leq 4$, the energy difference calculated between the ferromagnetic (FM) and antiferrimagnetic configurations indicates that the FM order is always preferable. Table I collects the local magnetic moments of $O_x/Fe_2/TiO_2/ATiO_3(001)$, which were calculated for the Fe atom, interfacial Ti-I and O-I and oxygen adatoms (O_{ad}). The number of adatoms varies in Table I from $x=0$ to $x=2$. We show the data for the most favored atomic configuration of each coverage $c\leq 1$. For $x=1$ the O_A configuration is preferable. When $x=2$ there are two oxygen adatoms which occupy the sites O_T and O_A above Ti and A, respectively. Considering the Fe magnetic moments, which all are significantly enhanced with respect to the Fe bulk value, one can notice that m_{Fe} increases with increasing c. For $P_\downarrow$, the Fe magnetic moment of $O_x/Fe/PTO$ is larger than that of $O_x/Fe/BTO$ (with one ex-

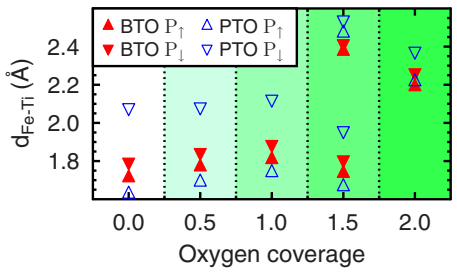

FIG. 7. (Color online) The distance between the Fe and Ti-I layers in $O_x/Fe_2/ATiO_3(001)$.

ception for $x=2$) and, vice versa, $m_{Fe}(PTO) < m_{Fe}(BTO)$ for $P_\uparrow$. As a result, the change in m_{Fe} due to the polarization reversal is always larger for PTO compared with the BTO system. For all x and both **P**, the O magnetic moments induced on O-I and O_{ad} are parallel to those of Fe. For the O adatoms at $x=1,2$ we obtained an averaged magnetic moment of 0.2 μ_B, which is two times larger than that of interfacial O from the TiO_2 layer. Reversal of P affects the O magnetic moments less significantly than m_{Fe} and m_{Ti}. We analyzed the magnetic moments of some energetically unfavored configurations. In particular, the energy splitting between BTO and PTO, seen in Fig. 2 at $c=1$, originates mostly from the magnetism of $O_2/Fe_2/BTO$, which is significantly suppressed for the two highly unexpected configurations AF and FF. The total magnetization of $O_2/Fe_2/BTO$, for instance, may drop below 0.1 μ_B per cell when both oxygen adatoms relax above Fe.

The hybridization between the $3d$ states of Fe and Ti leads to an induced magnetic moment on the Ti-I site, which is oriented opposite to m_{Fe}. This is shown in Table I. The antiferromagnetically oriented magnetic moment of interfacial Ti contributes significantly to ΔM. Surprisingly, for the $P_\downarrow$ state of $O_x/Fe/PTO$, we get $m_{Ti} \to 0$. This needs a careful analysis of the structure. In Fig. 7, we show the distance, $d_{Fe\text{-}Ti}$, between the Fe and Ti-I layers in $O_x/Fe_2/ATiO_3(001)$ for each coverage. When $c \leq 1$, the Fe-Ti distance is systematically shorter for $P_\uparrow$ and, therefore, the corresponding m_{Ti} is larger than that of the $P_\downarrow$ state. In $O_x/Fe/PTO$, the magnitude of $d_{Fe\text{-}Ti}$ increases noticeably for $P_\downarrow$, as shown in Fig. 7. This weakens the d-state hybridization of Fe and Ti leading to marginal m_{Ti}. For the coverage $c=1.5$, one oxygen adatom relaxed above Fe yields the second set of $d_{Fe\text{-}Ti}$, with the magnitudes ~0.6 Å larger than that of uncovered Fe. For $c=2$, when both Fe are covered by O adatoms we obtained again a single set of $d_{Fe\text{-}Ti}$. In the case of $c=1.5$ and $c=2$, the magnetic moment of Ti-I changes not so dramatically as the magnetic moments of a pair of covered Fe and its shortly distanced O adatom. For the former, we obtained a 1 μ_B reduction from ~3 to 2 μ_B per m_{Fe}, while the topmost O adatom above Fe shows the moment of ~0.5 μ_B. Meanwhile all other O adatoms of these configurations, which are labeled as O_A and O_T, show the magnetic moment of 0.12 μ_B or even less than 0.06 μ_B that happens at $c=2$ when O_A/O_T is positioned below the Fe layer. Since both high coverages $c=1.5$ and $c=2$ are energetically not preferable, we do not focus on their magnetic properties.

The magnetic contributions of each species of $O_x/Fe/ATiO_3(001)$ to the total magnetization change, ΔM, induced by the **P** reversal are shown in Fig. 8. We counted there the contributions from the two Fe atoms, one interfacial Ti, two O-I, and a number of oxygen adatoms. There are two oxygen adatoms for $c=1$ and one O adatom per cell for $c=0.5$. Figure 8 clearly illustrates the dissimilar behavior of BTO and PTO. For an uncovered ML Fe on BTO, we find that almost two-thirds of $\Delta M \approx 0.04$ μ_B comes from Ti-I while the two Fe atoms bring one-third only. With increasing $c \leq 1$, the Ti contribution to ΔM in this system gradually decreases whereas all ferromagnetically ordered Fe and O contribute >50%. As a result, ΔM in $O_x/Fe/BTO$ increases to the value of 0.25 μ_B per cell at $c=1$. In Fe/PTO with no oxygen adatoms, one half of its $\Delta M=1$ μ_B comes from Fe. In $O_x/Fe/PTO$, the **P**-induced change in its M follows the Fe proportion: first, ΔM reaches the 1.3 μ_B maximum at $c=0.5$ and then, with increasing c from 1/2 to 1, it diminishes below 0.9 μ_B. Nevertheless, the effect may result in rather strong ME coupling.

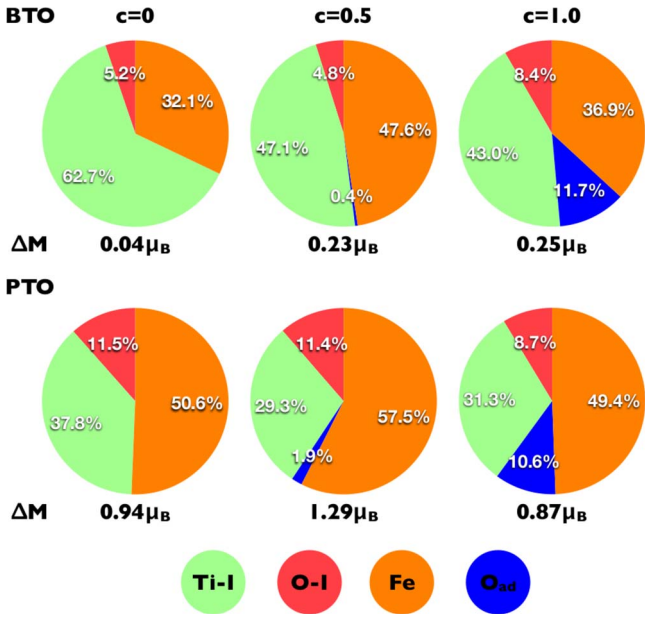

FIG. 8. (Color online) Relative contributions of each magnetic species to the magnetization change, ΔM, induced in $O_x/Fe_2/ATiO_3(001)$ (A=Ba,Pb and $x=0,1,2$) due to the polarization reversal. The contributions from the two Fe atoms, one interfacial Ti (Ti-I), two interfacial O (O-I) and oxygen adatoms (O_{ad}) were counted. There are two O adatoms for the coverage $c=1$ and one adatom for $c=0.5$. The total ΔM values are shown below each diagram.

In the top panel of Fig. 9 we show the total **M**, calculated including the interstitial contributions for the lowest energy configuration of $O_x/Fe_2/ATiO_3$ for each O coverage. There are the configurations A, AT, ATF, and ATFF obtained for $c=0.5$, 1, 1.5, and 2, respectively. The magnetization of uncovered Fe/PTO and Fe/BTO is also shown in Fig. 9. The increase in **M** seen for $c=0.5$ and $c=1$, as compared to that of $c=0$, is partially due to an induced magnetic moment of the O adatom, which is aligned parallel to the Fe magnetic moment. Besides, for $c=0.5$ and $c=1$, the Fe moment value is enhanced by the presence of the adatom. Contrarily, when the O adatom relaxes above Fe in the configurations ATF and

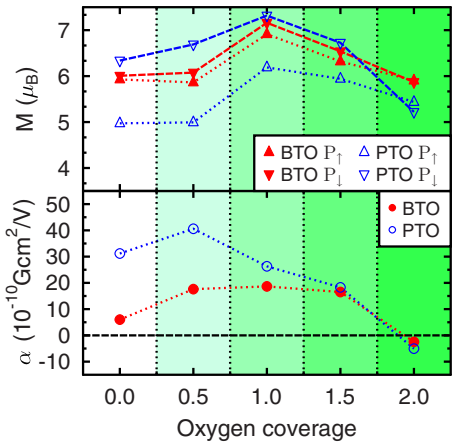

FIG. 9. (Color online) Total magnetization of the $O_x/Fe_2/ATiO_3(001)$ cell (A=Ba,Pb and $0<x<4$) is plotted as a function of oxygen coverage in the top panel. For each coverage the most favorable configuration was used. The corresponding magnetoelectric coupling coefficient is plotted in the lower panel.

ATFF, the Fe magnetic moment is decreased by $\sim 1\ \mu_B$. This is mostly due to a relatively short separation between the O adatom and Fe along [001]. As a result, the value of **M** gradually decreases with increasing $c>1$. For the magnetoelectric coupling the change in the magnetization induced by polarization reversal: $\Delta M = M(P_\downarrow) - M(P_\uparrow)$ is an important quantity. Previously, we have found[11] that for the uncovered 1 ML Fe on PTO (BTO) its $\Delta M \sim 1.2\ \mu_B$ ($\sim 0.1\ \mu_B$). Here it is obvious that in the case of O/Fe/BTO the magnitude of ΔM remains rather stable for O coverages <1.5 and then with further increase in c, $\Delta M \to 0$ at $c=2$. For the PTO substrate, the trends of ΔM computed for $c>1.5$ are similar to those of BTO. It should be kept in mind that the dense coverage of $c=2$ is unrealistic since the highest oxidation state of iron seen in Fe_2O_3 mimics the coverage $c=1.5$.

The interface ME coupling coefficient, α, can be evaluated as the ratio of the surface magnetization change $\mu_0 \Delta \mathbf{M}/S$ and the coercive field E_c, where S is the interface area. The experimental $E_c=10$ kV/cm and $E_c=33$ kV/cm were used for Fe/BTO and Fe/PTO, respectively. In Fig. 9, we plot the calculated α vs c. In general, α, as a function of c, follows the trends of ΔM. We find that the two systems obey almost the same strength of α when $1<c<1.5$. However, for the most favorable O coverage, $c=1$, the use of the highly polar PTO substrate may result in the largest ME effect. Niranjan *et al.*[14] reported that for the O-rich interface between magnetite and BTO, which formally corresponds to $c=2$, the value of α is smaller by a factor of 3, compared to that of the oxygen-free-type interface of Fe_3O_4. For a single Fe layer on BTO, we detect very similar trends of ME coupling seen in Fig. 9 comparing the results between the O coverage $c=2$ and $c=0$.

Since this work uses the local spin-density approximation to DFT, one can speculate that the model can incorrectly prescribe spin polarization to the p orbitals of oxygen adatom. Indeed, for any Fe-O system there are two competing phenomena: the electronic correlation and hybridization of their Fe $3d$ and O $2p$ orbitals. The electronic correlation effects can quantitatively contribute to the magnetic properties of ultrathin composite multiferroics. To deal with the on-site Coulomb correlations of $O_x/Fe/TiO_2$ more flexibly, it is worthwhile, therefore, to carry out more *ab initio* calculations beyond the conventional LDA.

IV. CONCLUSIONS

In summary, we present an *ab initio* study of the effect of oxidation on the strength of magnetoelectric coupling seen at the ferromagnet/ferroelectric interface in epitaxial multiferroics. The oxygen coverage, ranging between $c=0.5$ and two adsorbed O per Fe atom were simulated for $O_x/Fe_2/BaTiO_3(001)$ and $O_x/Fe_2/PbTiO_3(001)$ multiferroics. We suggest that oxygen adatoms may find their relaxed positions atop the Ba(Pb) and/or Ti sites. For $c>1$, the magnetic properties computed for the Fe layer gradually degrade with increasing O coverage. However, when $c<1.5$ the change in magnetization induced by polarization reversal is robust for all energetically preferable compositions. On the basis of our calculations we, therefore, suggest that intrinsic oxidation of biferroics may not significantly damage their magnetoelectricity. In the case of realistic oxygen coverage ($c=1$), we expect that the strength of magnetoelectric coupling remains rather strong for both MF systems under consideration.

ACKNOWLEDGMENTS

This work is supported by the *Sonderforschungsbereich* SFB 762, 'Functionality of Oxidic Interfaces.' M. Fechner is a member of the International Max Planck Research School for Science and Technology of Nanostructures.

*fechner@mpi-halle.mpg.de

[1] K. F. Wang, J. M. Liu, and Z. F. Ren, Adv. Phys. **58**, 321 (2009).
[2] H. Schmid, J. Phys.: Condens. Matter **20**, 434201 (2008).
[3] W. Eerenstein, M. Wiora, J. L. Prieto, J. F. Scott, and N. D. Mathur, Nature Mater. **6**, 348 (2007).
[4] S.-W. Cheong, Nature Mater. **6**, 927 (2007).
[5] F. Zavaliche, T. Zhao, H. Zheng, F. Straub, M. P. Cruz, P.-L. Yang, D. Hao, and R. Ramesh, Nano Lett. **7**, 1586 (2007).
[6] M. Dawber, K. M. Rabe, and J. F. Scott, Rev. Mod. Phys. **77**, 1083 (2005).
[7] D. Khomskii, Phys. **2**, 20 (2009).
[8] M. Fiebig, J. Phys. D: Appl. Phys. **38**, R123 (2005).
[9] J. M. Rondinelli, M. Stengel, and N. A. Spaldin, Nat. Nanotechnol. **3**, 46 (2008).
[10] C.-G. Duan, S. S. Jaswal, and E. Y. Tsymbal, Phys. Rev. Lett. **97**, 047201 (2006).
[11] M. Fechner, I. V. Maznichenko, S. Ostanin, A. Ernst, J. Henk, P. Bruno, and I. Mertig, Phys. Rev. B **78**, 212406 (2008).

[12] C. Yu, M. J. Pechan, S. Srivastava, C. J. Palmstrøm, M. Biegaslski, C. Brooks, and D. Schlom, J. Appl. Phys. **103**, 07B108 (2008).
[13] C.-G. Duan, J. P. Velev, R. F. Sabirianov, W. N. Mei, S. S. Jaswal, and E. Y. Tsymbal, Appl. Phys. Lett. **92**, 122905 (2008).
[14] M. K. Niranjan, J. P. Velev, C.-G. Duan, S. S. Jaswal, and E. Y. Tsymbal, Phys. Rev. B **78**, 104405 (2008).
[15] C. A. F. Vaz, J. Hoffman, A.-B. Posadas, and C. H. Ahn, Appl. Phys. Lett. **94**, 022504 (2009).
[16] G. Kresse and J. Furthmüller, Phys. Rev. B **54**, 11169 (1996).
[17] J. Hafner, J. Comput. Chem. **29**, 2044 (2008).
[18] M. Fechner, S. Ostanin, and I. Mertig, Phys. Rev. B **77**, 094112 (2008).
[19] D. Vanderbilt and R. D. King-Smith, Phys. Rev. B **48**, 4442 (1993).
[20] R. Resta, Rev. Mod. Phys. **66**, 899 (1994).
[21] H. J. Monkhorst and J. D. Pack, Phys. Rev. B **13**, 5188 (1976).
[22] R. Wu and A. Freeman, J. Magn. Magn. Mater. **127**, 327 (1993).
[23] P. Blonski, A. Kiejna, and J. Hafner, Surf. Sci. **590**, 88 (2005).
[24] M. Stengel, D. Vanderbilt, and N. A. Spaldin, Nature Mater. **8**, 392 (2009).